Title:

Expression dynamics of ARGONAUTE proteins during meiosis in Arabidopsis

Authors and affiliation:

Cecilia Oliver and German Martinez.

Department of Plant Biology, Uppsala BioCenter, Swedish University of Agricultural Sciences and Linnean Center for Plant Biology, Uppsala, Sweden

Corresponding authors:

Cecilia Oliver: cecilia.oliver.velasco@slu.se

German Martinez: german.martinez.arias@slu.se

ORCID information:

Cecilia Oliver: 0000-0002-5231-7910

German Martinez: 0000-0002-5215-0866

Abstract

Meiosis is a specialized cell division that is key for reproduction and genetic diversity in sexually reproducing plants. Recently, different RNA silencing pathways have been proposed to carry a specific activity during meiosis, but the pathways involved during this process remain unclear. Here, we explored the subcellular localization of different ARGONAUTE (AGO) proteins, the main effectors of RNA silencing, during male meiosis in *Arabidopsis thaliana* using immunolocalizations with commercially available antibodies. We detected the presence of AGO proteins associated with posttranscriptional gene silencing (AGO1, 2 and 5) in the cytoplasm or the nucleus, while AGOs associated with transcriptional gene silencing (AGO4 and 9) localized exclusively in the nucleus. These results indicate that the localization of different AGOs correlates with their predicted roles at the transcriptional and posttranscriptional levels and provide an overview of their timing and potential role during meiosis.

Introduction

Meiosis is a special type of cell division where one round of DNA synthesis is followed by two rounds of cell division, segregating homologous chromosomes during the first division and sister chromatids at the second division (Marston et al. 2004, Mercier et al. 2015). This process is key for the production of gametes and the reshuffling of the genetic information during sexual reproduction (Bolcun-Filas et al. 2018). The mechanisms regulating meiosis have been widely studied at the cellular, genetic, and molecular levels in a variety of organisms. In plants, more than 90 genes have been identified comprising

38 different meiotic processes that include double-strand break (DSB) formation,
39 chromosome segregation or meiotic recombination (Huang et al. 2019a). Intriguingly, in
40 the recent years it has been revealed that several of these processes involve the RNA
41 silencing machinery (Oliver et al. 2016, Underwood et al. 2018, Wei et al. 2012). Different
42 RNA silencing pathways are active during meiosis (Huang et al. 2020, Huang, et al.
43 2019a, Yelina et al. 2015). The miRNA affects chromatin condensation and the number
44 of chiasmas, while the RNA-directed DNA methylation (RdDM) pathways affects
45 chromatin condensation, the number of chiasmas and chromosome segregation (Oliver
46 et al. 2017, Oliver, et al. 2016). Moreover, the RdDM pathway protects euchromatic
47 regions from meiotic recombination (Yelina, et al. 2015). Additionally, *Arabidopsis* a non-
48 canonical RNA silencing pathway plays a role in double-strand break repair (Wei, et al.
49 2012). Moreover, meiocyte-specific sRNAs between 23-24 nts are positively correlated
50 with genes that have a meiocyte-preferential expression pattern (Huang, et al. 2019a),
51 which could correlate with the observed role of DNA methylation in the regulation of gene
52 expression in meiocytes (Walker et al. 2018). ARGONAUTE (AGO) proteins are the
53 effectors of the different RNA silencing pathways and have dedicated members that act
54 at the posttranscriptional or transcriptional levels. Here, we analyze the subcellular
55 localization of the main AGO proteins in Arabidopsis during the different meiosis stages,
56 which provides a confirmation of their activity during this process.

57

58 **Materials and Methods**

59 **Plant material**

60 Plants used for immunolocalization analysis were grown in a phytotron under long day
61 conditions (16-hour light/8-hour dark photoperiod), at 24-25 °C and 45% relative humidity.

62

63 **Bioinformatic analysis**

64 sRNA data was downloaded from the SRA repository project number PRJNA510650
65 (Huang et al. 2019b). sRNA alignments were performed using bowtie (Langmead et al.
66 2009) with the following parameters –t –v2 that allows 2 mismatches to the alignments.
67 Alignment files were subsequently analyzed in Galaxy (Afgan et al. 2018). For sRNA
68 categorization as miRNAs, sRNA libraries were aligned to individual indexes generated
69 for each genomic category and compared total sRNAs mapping to the TAIR10
70 chromosome sequences. The miRbase version 22.1 (https://www.mirbase.org/) was
71 used for miRNA alignments (Kozomara et al. 2019). Transcriptomic data corresponds to
72 the CATMA arrays data from GEO accessions GSE10229 and GSE13000 (Libeau et al.
73 2011). CATMA array data was extracted using the CATdb database
74 (http://urgv.evry.inra.fr/cgi-bin/projects/CATdb/catdb_index.pl) were normalized data was
75 extracted for both GSE10229 (http://urgv.evry.inra.fr/cgi-
76 bin/projects/CATdb/consult_expce.pl?experiment_id=195) and GSE13000
77 (http://urgv.evry.inra.fr/cgi-bin/projects/CATdb/consult_expce.pl?experiment_id=46).

78

79 **Cytology**

80 Immunolocalization on meiotic nuclei were carried out by squash technique as was
81 previously described by Manzanero et al. (2000) with some modifications (Oliver et al.,

82 2013). Two bioreplicates constituted by young flower buds from five different plants, were
83 analyzed. Young flower buds were fixed for 20 min in freshly prepared 4 % (w/v)
84 paraformaldehyde, 0.1 % (v/v) Triton X-100 in phosphate-buffered saline (PBS, pH 7.3).
85 Flower buds were then washed at room temperature for 30 min in PBS that was changed
86 twice. Buffer was removed before incubation at 37ºC during 20–40 min with an enzyme
87 mixture of 1 % pectinase, 1 % cellulase and 1 % cytohelicase (w/v) (Sigma), dissolved in
88 PBS. Buds, immersed in a small volume of PBS, were transferred to slides with a Pasteur
89 pipette, macerated with a needle and squashed between a glass slide and cover slip.
90 After freezing in liquid nitrogen, the cover slips were removed and the slides were
91 transferred immediately into PBS. Prior to immunostaining experiments the slides were
92 washed twice in PBS, 0.1 % (v/v) Triton X-100 for 5 min each. To avoid non-specific
93 antibody binding, slides were incubated for 30 min in PBS with 1 % BSA (w/v) and 0.1 %
94 Triton X-100 at room temperature. The incubation with the primary antibody was carried
95 out in a humidified chamber. The primary antibodies used were rabbit anti-AGO1 (1:200
96 AS09 527), -AGO2 (1:100, AS13 2682), -AGO5 (1:100, AS10 671), -AGO4 (1:100, AS09
97 617), -AGO6 (1:50, AS10 672), -AGO9 (1:100, AS10 673) and -AGO10 (1:50, AS15 3071)
98 antibodies from Agrisera. All the primary antibodies were diluted in PBS, 1 % BSA, 0.1 %
99 Triton X-100. After overnight incubation at 4ºC and washing for 15 min in PBS with 0.1 %
100 Triton X-100, the slides were incubated for 1 h at room temperature with goat anti-rabbit
101 IgG H&L Alexa Fluor 568 conjugated (1:200; ab175471; Abcam) diluted in 1 % BSA, 0.1
102 % Triton X-100 in PBS. Slides were then washed in PBS, 0.1 % Triton X-100, before they
103 were stained the DAPI, 1 µg/ml during 20-30 min and finally mounting with antifading
104 medium (0.2% n-propyl Gallete, 0.1% DMSO, 90% glycerol in PBS). Fluorescent signals

105 were observed using an epifluorescence microscope Zeiss AxioScope A1. Images were
106 captured with AxioCam ICc5 camera and were analyzed and processed with ImageJ and
107 Affinity Photo software.

108

109 **Results**

110 To discern the level of expression of RNA silencing components in meiocytes, we
111 analyzed their expression from publicly available microarray datasets (Libeau, et al. 2011)
112 (Figure 1 and Supplementary Methods). Overall, several components from the RNA
113 silencing pathways were preferentially expressed in meiocytes compared to somatic
114 tissues (Figure 1A), including the AGO proteins AGO4, 5 and 10, the Dicer-like (DCL)
115 proteins DCL1, 3 and 4 or the sRNA methyltransferase HEN1. This indicated that different
116 PTGS (AGO5, DCL1 and DCL4) and TGS (AGO4 and DCL3) pathways might be
117 especially active during meiosis. Previous analysis (Huang, et al. 2019a) have shown that
118 TE-derived sRNAs accumulate to relatively high levels in meiocytes and that certain
119 miRNAs like miR845 are active before the microspore stage (Borges et al. 2018).
120 Although miRNAs were not globally enriched in meiocytes (Figure 1B), several miRNAs
121 were strongly upregulated including miR839, miR780.2, miR780.1, miR157, miR172,
122 miR166 and miR860, which are important regulators of several transcription factor
123 families (Figure 1C, Supplementary Figure 1 and Supplementary Table 2). In summary,
124 transcriptomic and sRNA sequencing analysis supported the notion that the RNA
125 silencing machinery might have a meiocyte-specific activity.

126

127 Although transcriptomic analysis is important to infer the activity of the different RNA
128 silencing pathways in meiocytes, this analysis provides a steady image of this tissue and
129 ignores, for example, its dynamism during meiosis. To understand the subcellular
130 localization and dynamics of the different AGO proteins during meiosis, we performed
131 immunolocalizations of the AGO proteins that had commercially available antibodies
132 (Agrisera, AGO1, 2, 4, 5, 6, 9 and 10, Figure 2 and Supplementary Methods). During
133 meiosis all AGOs but AGO6 and AGO10 could be detected. In detail, AGO1 and its
134 paralogs AGO2 and AGO5 displayed a similar localization and expression pattern during
135 the first meiotic stages (Figure 2A, 2B, 2C). The three proteins were located mainly in the
136 cytoplasm, similar to their localization in somatic tissues (Bologna et al. 2018, Ye et al.
137 2012). From the leptotene to the diplotene stage these three AGO proteins formed
138 cytoplasmic granules (Figure. 2A1, 2B1, 2C1). In somatic tissues, cytoplasmic bodies are
139 involved in the degradation and translation arrest of mRNAs (Maldonado-Bonilla 2014).
140 In mammals, AGO proteins localize in P-bodies where they mediate the translational
141 repression of their target mRNAs (Liu et al. 2005). The localization pattern observed for
142 AGO1, 2 and 5 might indicate a similar role of RNA silencing in the posttranscriptional
143 regulation of mRNAs, a process that is known to take place in other organisms like
144 mammals (Yao et al. 2015).

145

146 Despite the similarities between the accumulation during meiosis, AGO1, 2 and 5, they
147 showed differences in their dynamics during meiosis. For example, AGO1 condensates
148 around the nuclear envelope at diplotene (Figure 2A4) but after this stage, it showed a
149 disperse accumulation (Figure 2A5). This location during cell division could be related

150 with the known AGO1 association with the endoplasmic reticulum (Li et al. 2013), as when
151 the nuclear envelope disassembles it reorganizes in vacuoles around the bivalents
152 (Marston, et al. 2004, Mercier, et al. 2015). AGO5 displayed a similar pattern of
153 subcellular localization to AGO1, although its localization at cytoplasmic bodies
154 disappeared at diplotene (Figure 2B4). On the other hand, AGO2 showed a dual
155 localization in the cytoplasm and in the nucleus (Figure 2C1-4) and was not detectable
156 after metaphase I (Figure 2C5-6). Both its nucleocytoplasmic localization and timing of
157 expression are in line with its known role in double strand break (DSB) repair, which takes
158 place during the first meiotic stages (Oliver et al. 2014, Wei, et al. 2012). Nevertheless,
159 AGO2 expression pattern was recapitulated after the second meiotic division (Figure
160 2C7), indicating that it might serve other roles in parallel to its function in DSB repair
161 during meiosis.

162

163 On the other hand, the TGS/RdDM-associated AGO proteins, AGO4 and AGO9, were
164 located in the nuclei during all meiotic stages (Figure 2D and E). Exceptionally, at
165 metaphase I, when the nuclear envelope dissolves, both proteins showed a dispersed
166 accumulation. This is in accordance with the known role of the RdDM pathway in
167 regulating DNA methylation during meiosis (Walker, et al. 2018). Meiocytes have the
168 lowest CHH methylation values of all the reproductive nuclei analyzed, but its activity is
169 needed for the regulation of gene expression (Walker, et al. 2018). We detected a low
170 accumulation of AGO4 and 9 after metaphase I (Figure 2D5-6 and 2E5-6), which might
171 partially cause this reduction in CHH methylation. Interestingly, we observed that AGO9
172 displayed a localization pattern compatible with a preference for heterochromatic regions

173 at pachytene. This localization might explain the known role of AGO9 on the dissolution
174 of interlocks during meiosis (Oliver, et al. 2014).

175

176 **Discussion**

177 In summary, our results provide an overview of the subcellular localization, timing and
178 potential role of different RNA silencing pathways during meiosis. Furthermore, our work
179 complements previous analysis that analyzed RNA silencing activity in meiocytes, and
180 opens the door for future molecular analysis of the specific role of AGO proteins during
181 specific meiosis stages, which are technically challenging at the moment.

182

183 **Author contribution statement:** C.O and G.M. design the experiments and wrote the
184 manuscript. C.O. performed the experiments and analyzed the data. G.M. analyzed the
185 bioinformatic data.

186

187 **Acknowledgements**

188 The authors thank SLU, the Carl Tryggers Foundation (CTS 17-305 and CTS 18-251),
189 the Swedish Research Council (VR 2016-05410) and the Knut and Alice Wallenberg
190 Foundation (KAW 2019-0062) for supporting research in the Martinez group. The data
191 handling was enabled by resources provided by the Swedish National Infrastructure for
192 Computing (SNIC) at UPPMAX partially funded by the Swedish Research Council through
193 grant agreement no. 2018-05973.

194

195 **References:**

196 Afgan E, Baker D, Batut B, van den Beek M, Bouvier D, Čech M, Chilton J, Clements D,
197 Coraor N, Grüning BA, Guerler A, Hillman-Jackson J, Hiltemann S, Jalili V, Rasche
198 H, Soranzo N, Goecks J, Taylor J, Nekrutenko A, Blankenberg D (2018) The
199 Galaxy platform for accessible, reproducible and collaborative biomedical
200 analyses: 2018 update. Nucleic Acids Research 46:W537-W544

201 Bolcun-Filas E, Handel MA (2018) Meiosis: the chromosomal foundation of reproduction.
202 Biol Reprod 99:112-126

203 Bologna NG, Iselin R, Abriata LA, Sarazin A, Pumplin N, Jay F, Grentzinger T, Dal Peraro
204 M, Voinnet O (2018) Nucleo-cytosolic Shuttling of ARGONAUTE1 Prompts a
205 Revised Model of the Plant MicroRNA Pathway. Mol Cell 69:709-719 e705

206 Borges F, Parent JS, van Ex F, Wolff P, Martinez G, Kohler C, Martienssen RA (2018)
207 Transposon-derived small RNAs triggered by miR845 mediate genome dosage
208 response in Arabidopsis. Nat Genet 50:186-192

209 Huang J, Wang C, Li X, Fang X, Huang N, Wang Y, Ma H, Wang Y, Copenhaver GP
210 (2020) Conservation and Divergence in the Meiocyte sRNAomes of Arabidopsis,
211 Soybean, and Cucumber. Plant Physiol 182:301-317

212 Huang J, Wang C, Wang H, Lu P, Zheng B, Ma H, Copenhaver GP, Wang Y (2019a)
213 Meiocyte-Specific and AtSPO11-1-Dependent Small RNAs and Their Association
214 with Meiotic Gene Expression and Recombination. Plant Cell 31:444-464

215 Huang JY, Wang C, Wang HF, Lu PL, Zheng BL, Ma H, Copenhaver GP, Wang YX
216 (2019b) Meiocyte-Specific and AtSPO11-1-Dependent Small RNAs and Their

217 Association with Meiotic Gene Expression and Recombination. Plant Cell 31:444-
218 464
219 Kozomara A, Birgaoanu M, Griffiths-Jones S (2019) miRBase: from microRNA sequences
220 to function. Nucleic Acids Research 47:D155-D162
221 Langmead B, Trapnell C, Pop M, Salzberg SL (2009) Ultrafast and memory-efficient
222 alignment of short DNA sequences to the human genome. Genome Biol 10:R25
223 Li S, Liu L, Zhuang X, Yu Y, Liu X, Cui X, Ji L, Pan Z, Cao X, Mo B, Zhang F, Raikhel N,
224 Jiang L, Chen X (2013) MicroRNAs inhibit the translation of target mRNAs on the
225 endoplasmic reticulum in Arabidopsis. Cell 153:562-574
226 Libeau P, Durandet M, Granier F, Marquis C, Berthome R, Renou JP, Taconnat-Soubirou
227 L, Horlow C (2011) Gene expression profiling of Arabidopsis meiocytes. Plant Biol
228 (Stuttg) 13:784-793
229 Liu J, Valencia-Sanchez MA, Hannon GJ, Parker R (2005) MicroRNA-dependent
230 localization of targeted mRNAs to mammalian P-bodies. Nat Cell Biol 7:719-723
231 Maldonado-Bonilla LD (2014) Composition and function of P bodies in Arabidopsis
232 thaliana. Front Plant Sci 5:201
233 Manzanero S, Arana P, Puertas MJ, Houben A (2000) The chromosomal distribution of
234 phosphorylated histone H3 differs between plants and animals at meiosis.
235 Chromosoma 109:308-317
236 Marston AL, Amon A (2004) Meiosis: cell-cycle controls shuffle and deal. Nat Rev Mol
237 Cell Biol 5:983-997
238 Mercier R, Mezard C, Jenczewski E, Macaisne N, Grelon M (2015) The molecular biology
239 of meiosis in plants. Annu Rev Plant Biol 66:297-327

240 Oliver C, Pradillo M, Corredor E, Cuñado N (2013) The dynamics of histone H3
241 modifications is species-specific in plant meiosis. Planta 238:23-33
242 Oliver C, Pradillo M, Jover-Gil S, Cunado N, Ponce MR, Santos JL (2017) Loss of function
243 of Arabidopsis microRNA-machinery genes impairs fertility, and has effects on
244 homologous recombination and meiotic chromatin dynamics. Sci Rep 7:9280
245 Oliver C, Santos JL, Pradillo M (2014) On the role of some ARGONAUTE proteins in
246 meiosis and DNA repair in Arabidopsis thaliana. Frontiers in Plant Science 5
247 Oliver C, Santos JL, Pradillo M (2016) Accurate Chromosome Segregation at First Meiotic
248 Division Requires AGO4, a Protein Involved in RNA-Dependent DNA Methylation
249 in Arabidopsis thaliana. Genetics 204:543-553
250 Underwood CJ, Choi K, Lambing C, Zhao X, Serra H, Borges F, Simorowski J, Ernst E,
251 Jacob Y, Henderson IR, Martienssen RA (2018) Epigenetic activation of meiotic
252 recombination near Arabidopsis thaliana centromeres via loss of H3K9me2 and
253 non-CG DNA methylation. Genome Res 28:519-531
254 Walker J, Gao H, Zhang J, Aldridge B, Vickers M, Higgins JD, Feng X (2018) Sexual-
255 lineage-specific DNA methylation regulates meiosis in Arabidopsis. Nat Genet
256 50:130-137
257 Wei W, Ba Z, Gao M, Wu Y, Ma Y, Amiard S, White CI, Rendtlew Danielsen JM, Yang
258 YG, Qi Y (2012) A role for small RNAs in DNA double-strand break repair. Cell
259 149:101-112
260 Yao CC, Liu Y, Sun M, Niu MH, Yuan QQ, Hai YA, Guo Y, Chen Z, Hou JM, Liu Y, He ZP
261 (2015) MicroRNAs and DNA methylation as epigenetic regulators of mitosis,
262 meiosis and spermiogenesis. Reproduction 150:R25-R34

263 Ye R, Wang W, Iki T, Liu C, Wu Y, Ishikawa M, Zhou X, Qi Y (2012) Cytoplasmic assembly
264 and selective nuclear import of Arabidopsis Argonaute4/siRNA complexes. Mol
265 Cell 46:859-870
266 Yelina NE, Lambing C, Hardcastle TJ, Zhao X, Santos B, Henderson IR (2015) DNA
267 methylation epigenetically silences crossover hot spots and controls chromosomal
268 domains of meiotic recombination in Arabidopsis. Genes Dev 29:2183-2202

269

270 **Figure legends:**

271 **Figure 1. Analysis of the expression in meiocytes of different RNA silencing and**
272 **epigenetic pathways components and analysis of miRNA accumulation in**
273 **meiocytes. A.** Heat map of the expression values of RNA silencing and epigenetic
274 pathways components in meiocyte microarray experiments. Expression values are
275 represented as the normalized log2 ratio of the comparison meiocyte/control tissue. **B.**
276 Global accumulation of miRNAs in leaves and meiocytes samples from public datasets
277 normalized to reads per million. **C.** Accumulation values of miRNAs enriched in meiocyte
278 sRNA libraries. Enrichment was considered only for miRNAs accumulating more than 2-
279 fold in meiocytes and with a p-value<0.05.

280

281 **Figure 2. Immunolocalization of AGO1 (A), AGO5 (B), AGO2 (C), AGO4 (D) and**
282 **AGO9 (E) at different representative meiotic stages in Arabidopsis meiocytes.**
283 Leptotene (A1, B1, C1, D1, E1); Zygotene (A2, B2, C2, D2, E2); Pachytene (A3, B3, C3,
284 D3, E3); Diplotene (A4, B4, C4, D4, E4); Diakinesis (B5), Metaphase I (A5, C5, D5, E5)

285 Prophase II (A6, B6, D6, E6); Metaphase II (C6); Tetrad (A7, B7, C7, D7, E7).
286 Immunostaining with antibodies is shown in red, counterstaining with DAPI is shown in
287 grey. Bar indicates 10 µm.

288

289 **Supplementary Figure 1.** Predicted and confirmed targets of miRNA families
290 significantly upregulated in meiocytes.

291

292 **Supplementary Table 1.** Raw values of normalized log2-ratio expression values for
293 selected genes in meiocytes microarray data.

294

295 **Supplementary Table 2.** Raw values of miRNA accumulation in meiocytes and leaf
296 sRNA libraries.

Figure 1

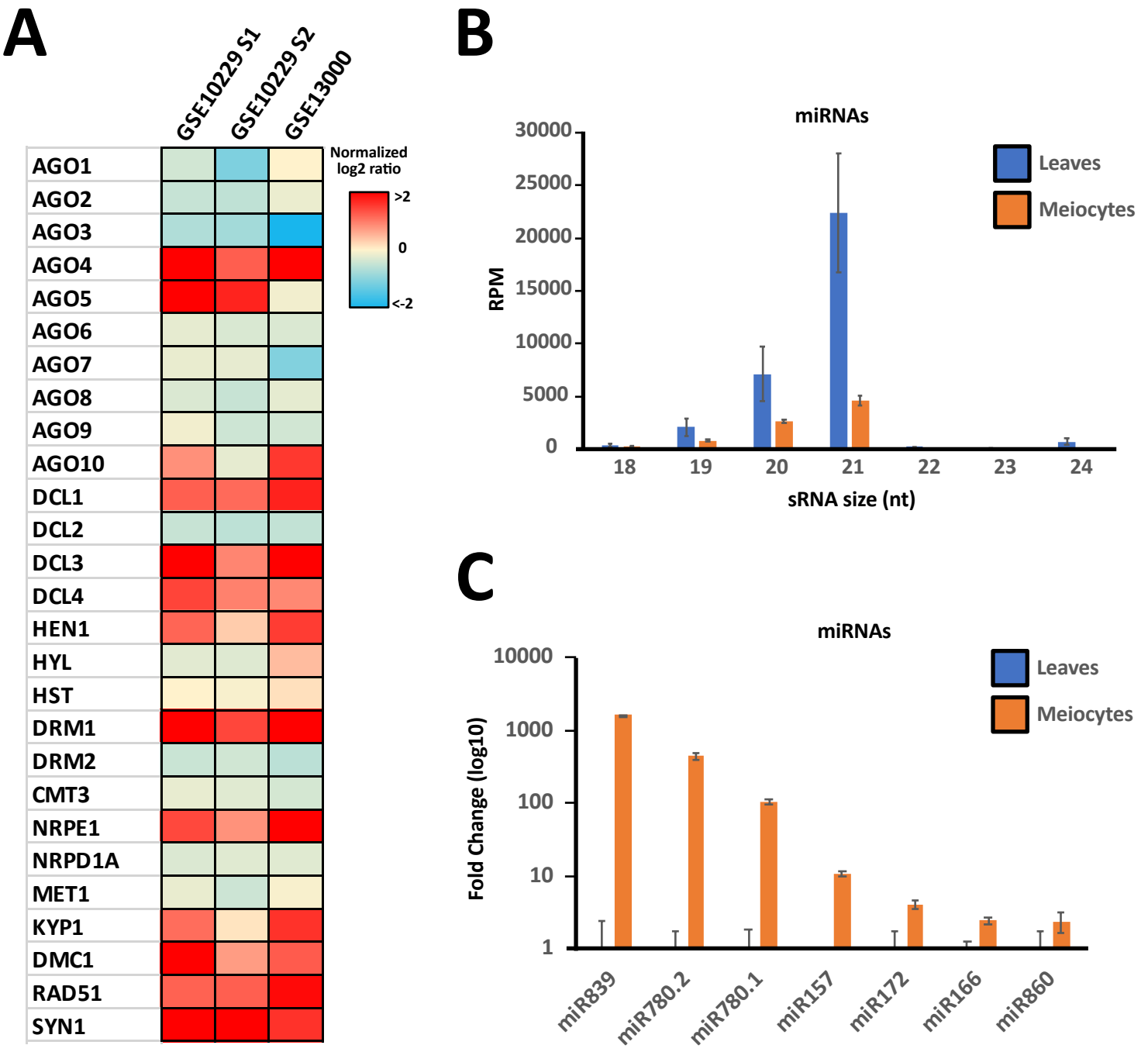
A
GSE10229 S1
GSE10229 S2
GSE13000
Normalized log2 ratio
>2
0
<-2
AGO1
AGO2
AGO3
AGO4
AGO5
AGO6
AGO7
AGO8
AGO9
AGO10
DCL1
DCL2
DCL3
DCL4
HEN1
HYL
HST
DRM1
DRM2
CMT3
NRPE1
NRPD1A
MET1
KYP1
DMC1
RAD51
SYN1
B
miRNAs
RPM
30000
25000
20000
15000
10000
5000
0
18
19
20
21
22
23
24
sRNA size (nt)
Leaves
Meiocytes
C
miRNAs
Fold Change (log10)
10000
1000
100
10
1
miR839
miR780.2
miR780.1
miR157
miR172
miR166
miR860
Leaves
Meiocytes

Figure 2.

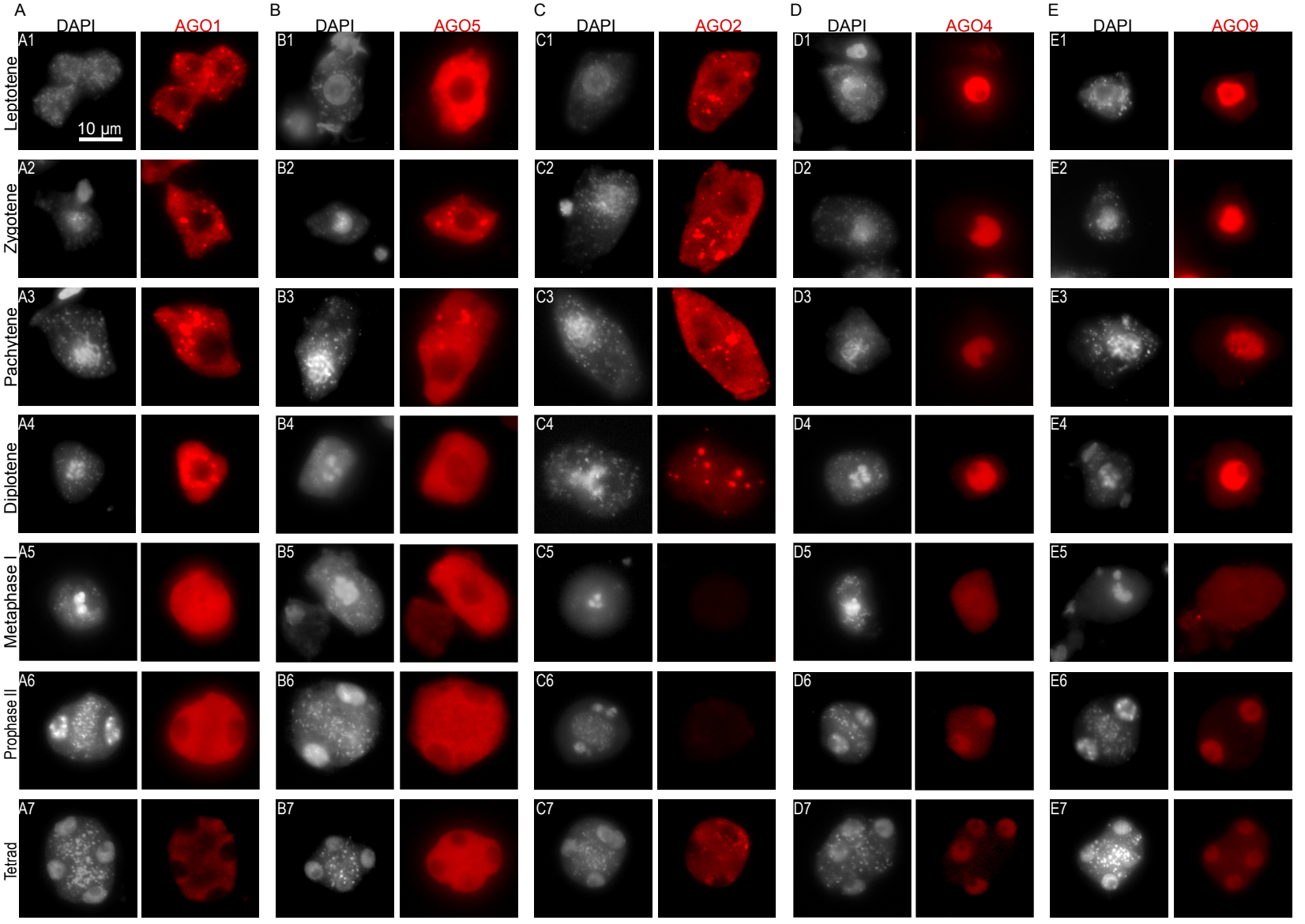
A
DAPI
AGO1
B
DAPI
AGO5
C
DAPI
AGO2
D
DAPI
AGO4
E
DAPI
AGO9
Leptotene
Zygotene
Pachytene
Diplotene
Metaphase I
Prophase II
Tetrad
A1
A2
A3
A4
A5
A6
A7
B1
B2
B3
B4
B5
B6
B7
C1
C2
C3
C4
C5
C6
C7
D1
D2
D3
D4
D5
D6
D7
E1
E2
E3
E4
E5
E6
E7
10 µm